

Comparison of (+)-¹¹C-McN5652 and ¹¹C-DASB as Serotonin Transporter Radioligands Under Various Experimental Conditions

Zsolt Szabo, MD, PhD¹; Una D. McCann, MD²; Alan A. Wilson, PhD³; Ursula Scheffel, PhD¹; Taofeek Owonikoko, MD¹; William B. Mathews, PhD¹; Hayden T. Ravert, PhD¹; John Hilton, PhD¹; Robert F. Dannals, PhD¹; and George A. Ricaurte, MD, PhD⁴

¹Division of Nuclear Medicine, Department of Radiology and Radiological Science, The Johns Hopkins School of Medicine, Baltimore, Maryland; ²Department of Psychiatry and Behavioral Science, The Johns Hopkins School of Medicine, Baltimore, Maryland; ³Vivian Rakoff PET Center, Center for Addiction and Mental Health, The University of Toronto, Toronto, Ontario, Canada; and ⁴Department of Neurology, The Johns Hopkins School of Medicine, Baltimore, Maryland

There has been considerable interest in the development of a PET radioligand selective for the serotonin (5-hydroxytryptamine [5-HT]) transporter (SERT) that can be used to image 5-HT neurons in the living human brain. The most widely used SERT radiotracer to date, *trans*-1,2,3,5,6,10- β -hexahydro-6-[4-(methylthio)phenyl]pyrrolo-[2,1-*a*]isoquinoline ((+)-¹¹C-McN5652), has been successful in this regard but may have some limitations. Recently, another promising SERT radiotracer, 3-¹¹C-amino-4-(2-dimethylaminomethylphenylsulfanyl)benzonitrile (¹¹C-DASB), has been described. The purpose of this study was to compare and contrast (+)-¹¹C-McN5652 and ¹¹C-DASB under various experimental conditions. **Methods:** Radioligand comparisons were performed in a control baboon, a baboon with reduced SERT density ((\pm)-3,4-methylenedioxymethamphetamine [MDMA] lesion), and a baboon with reduced SERT availability (paroxetine pretreatment). Under each of these experimental conditions, repeated (triplicate) PET studies were performed with each ligand. **Results:** Both radiotracers bound preferentially in brain regions known to contain high SERT density. For both ligands, there was a high correlation between the amount of regional brain ligand binding and the known regional brain concentration of SERT. Binding of both ligands was decreased after MDMA neurotoxicity (reduced SERT density), and (+)-¹¹C-McN5652 and ¹¹C-DASB were comparably effective in detecting reduced SERT density after MDMA-induced 5-HT neurotoxicity. Pretreatment with paroxetine dramatically altered the metabolism and kinetics of both tracers and appeared to displace both ligands primarily from regions with high SERT density. Compared with (+)-¹¹C-McN5652, ¹¹C-DASB had higher brain activity and a faster washout rate and provided greater contrast between subcortical and cortical brain regions. **Conclusion:** ¹¹C-DASB and (+)-¹¹C-McN5652 are suitable as PET ligands of the SERT and for detecting MDMA-induced 5-HT neurotoxicity. ¹¹C-DASB may offer some advantages. Additional

studies are needed to further characterize the properties and capabilities of both ligands in health and disease.

Key Words: PET; serotonin; transporters; paroxetine; (\pm)-3,4-methylenedioxymethamphetamine

J Nucl Med 2002; 43:678–692

The brain serotonin (5-HT) system has been implicated in several neuropsychiatric conditions, including major depression, anxiety, obsessive compulsive disorder, and schizophrenia. Because of the perceived importance of the brain 5-HT system in these diseases, as well as a variety of normal brain functions (e.g., appetite, sleep), there has been considerable interest in developing neuroimaging techniques that permit assessment of 5-HT neurons in the living human brain. To this end, several research teams have developed and evaluated various SPECT and PET radiotracers for measurements of various components of the brain 5-HT system (1–6). With regard to PET, a series of radioligands showing high binding to the 5-HT transporter (SERT) *in vitro* have been evaluated, but most have been found to have insufficient specificity or selectivity for the SERT *in vivo* (7).

To date, one of the more promising PET SERT radioligands identified is *trans*-1,2,3,5,6,10- β -hexahydro-6-[4-(methylthio)phenyl]pyrrolo-[2,1-*a*]isoquinoline ((+)-¹¹C-McN5652). (+)-¹¹C-McN5652 binds selectively to the SERT, and its regional distribution of binding in humans correlates well with the known distribution of the SERT in human brain (8–10). In addition, studies in baboons and humans exposed to the brain 5-HT neurotoxin, (\pm)-3,4-methylenedioxymethamphetamine (MDMA), show significant reductions in (+)-¹¹C-McN5652 binding (11–13). However, usefulness of (+)-¹¹C-McN5652 may be limited by its nonspecific binding and slow release from specific binding sites (14,15).

Received Aug. 29, 2001; revision accepted Jan. 16, 2002.
For correspondence or reprints contact: George A. Ricaurte, MD, PhD, Department of Neurology, Johns Hopkins Medical Institutions, 5501 Hopkins Bayview Circle, Baltimore, MD 21224.
E-mail: Ricaurte@jhmi.edu

There have been recent reports that an alternative SERT radioligand, 3-¹¹C-amino-4-(2-dimethylaminomethylphenylsulfanyl)benzotrile (¹¹C-DASB), holds promise for use as a SERT PET ligand (16,17). Preclinical studies indicate that, like (+)-¹¹C-McN5652, ¹¹C-DASB has high affinity and selectivity for the SERT in vitro and that, in vivo, it shows saturable and selective binding to the SERT in rodents. Also, damage of 5-HT axon terminals with the neurotoxin *p*-chloroamphetamine is associated with significant reductions in ¹¹C-DASB binding in vivo in rodents, and low concentrations of radioactive metabolites in rat brain relative to the parent compound (17) suggest that this radioligand holds significant potential for use in evaluating the status of the brain SERT in humans. Notably, initial PET studies in humans (18) indicate that ¹¹C-DASB has highly suitable characteristics for evaluating the status of the SERT in clinical settings and that ¹¹C-DASB can successfully detect SERT occupancy by paroxetine and citalopram (19).

The purpose of this study was to compare (+)-¹¹C-McN5652 and ¹¹C-DASB as PET ligands of the SERT in nonhuman primates. In particular, we sought to (a) compare binding characteristics of both radioligands to the SERT in a saline-treated baboon (normal SERT density), (b) compare the ability of the 2 radioligands to detect reductions in SERT density induced by the selective 5-HT neurotoxin MDMA, (c) evaluate the capability of both ligands to detect reduced SERT availability after pretreatment with paroxetine, and (d) determine how binding parameters of the 2 radioligands correlate with direct measures of brain 5-HT axonal markers measured *ex vivo*.

MATERIALS AND METHODS

Animals

Five *Papio anubis* baboons were used for these studies. Two of the baboons (males) were used for PET studies with (+)-¹¹C-McN5652 and ¹¹C-DASB; the other 3 served as control animals for the neurochemical studies of 5-HT axonal markers, including the SERT. Of the 2 baboons used in the PET studies, 1 was a saline-treated baboon (11 y old; weight, 24 kg). This animal underwent PET studies with each ligand on 3 separate occasions to compare binding characteristics of both radioligands to the SERT at baseline (normal SERT density). The same baboon then underwent 3 additional PET studies with each radioligand after treatment with a blocking dose of paroxetine to evaluate the capability of both ligands to detect reduced SERT availability. Another baboon (12 y old; weight, 25 kg) underwent 3 PET studies after administration of neurotoxic doses of MDMA to compare the ability of the 2 radioligands to detect reductions in SERT density caused by MDMA-induced 5-HT neurotoxicity.

Drug Treatment

As in previous studies, (13,20,21), MDMA was given at a dose of 5 mg/kg daily for 4 consecutive days to lesion 5-HT systems. However, the MDMA-treated baboon used in this study underwent 2 such 4-d MDMA regimens, one 17 mo and another 7 mo before initiation of the PET studies. The rationale behind the use of a baboon that received 2 separate MDMA treatments was to ensure that this animal had marked reductions in 5-HT axonal markers,

including SERT density. Shortly on completion of the PET studies (3 d later), the MDMA-treated animal was killed for direct in vitro measurement of indices of brain 5-HT axons, including the SERT, to be correlated with PET findings. Paroxetine studies were performed on the baboon treated previously with saline on 3 separate days, after pretreatment with 10 mg/kg paroxetine (either 10 mg/kg intravenously 60 min before tracer administration or 5 mg intramuscularly \times 2, the night before and 60 min before PET imaging). The latter paroxetine regimen was used to avoid use of a high bolus dose and to ensure near-maximal SERT blockade at the time of tracer injection.

Overall Design

Before PET imaging, animals were fasted for 12 h. Anesthesia was induced with 20 mL Saffan (Pitman-Moore, Middlesex, U.K.), a combination of alfaxalone and alfadolone acetate, intramuscularly and maintained with a constant infusion of Saffan at a rate of 55–70 mL/h. Saffan was diluted with isotonic saline in a ratio of Saffan:saline = 1:4. Circulatory volume was maintained by infusion of isotonic saline. Animals were intubated during PET studies, and heart rate, blood pressure, oxygen saturation, and core temperature were monitored continuously.

PET studies of the saline-treated, MDMA-treated, and paroxetine-pretreated baboon were conducted on 3 separate occasions at 3- to 4-wk intervals. On each of these occasions, animals were usually first scanned with (+)-¹¹C-McN5652 and then (at least 2 h later) with ¹¹C-DASB so that direct comparisons of the 2 radioligands could be made (i.e., minimizing variance created by conducting scans on separate days). On some occasions, ¹¹C-DASB was injected before (+)-¹¹C-McN5652, always at least 60 min after induction of anesthesia. The purpose of obtaining 3 scans with each ligand under each experimental condition (saline treatment [normal SERT density], after MDMA lesion [reduced SERT density], and after pretreatment with paroxetine [reduced SERT availability]) was to test reproducibility of the imaging findings and to allow statistical comparison of the binding data under each condition. Paroxetine studies were performed on 3 separate days, after pretreatment with 10 mg/kg paroxetine (either 10 mg/kg intravenously 60 min before tracer administration or 5 mg intramuscularly \times 2 the night before and 60 min before PET imaging). Given that these are high doses of paroxetine, near-maximal SERT occupancy would be anticipated after either paroxetine regimen.

MRI Protocol

To ensure reproducibility of positioning during the repeated PET studies, a custom-made face mask (TRU-SCAN, Annapolis, MD) was fitted to the baboon's head, which was then attached to the head holder during the PET scans. The canthomeatal line served as a reference for the PET studies. In each animal, 2 MRI sequences were obtained using a Signa 1.5-T scanner (General Electric Medical Systems, Milwaukee, WI). The first sequence was a set of T1-weighted scout images with the following parameters: repetition time (TR) = 500 ms; echo time (TE) = 20 ms; 5-mm slice thickness with no gap; 128 \times 256 matrix; and 1 excitation. The second sequence was an axial spin-density/T1-weighted 3-dimensional volumetric scan using radiofrequency spoiled gradient (SPGR) echoes. The parameters were as follows: TR = 35 ms; TE = 5 ms; flip angle = 45°; 1.5-mm effective slice thickness; no gap; 124 slices with in-plane 192 \times 256 matrix; 15-cm field of view; and 1 excitation. The purpose of the SPGR sequence was to ensure precise positioning and repositioning of the animals during multiple studies and to achieve image registration with PET for localization of the structures of interest.

PET Protocol

An Advance PET camera (General Electric) with an axial resolution (full width at half maximum) of 5.8 mm and an in-plane resolution of 5.4 mm was used for image acquisition. This scanner acquires 35 simultaneous slices of 4.25-mm thickness, enclosing a total longitudinal field of view of 15 cm. A transmission scan was obtained with twin 370-MBq (10 mCi) ^{68}Ge pin sources for 10 min and was used for attenuation correction of the subsequent emission PET scans. (+)- ^{11}C -McN5652 and ^{11}C -DASB were prepared according to published methods (17,22). Two PET studies were performed on every occasion: 1 with 555 MBq (15 mCi) (+)- ^{11}C -McN5652 and the other with 555 MBq ^{11}C -DASB. The time difference between the injections was 120 min. Specific activities ranged between 185 and 733 MBq/mmol (5,000 and 19,800 Ci/mmol; average, 354 MBq/mmol [9,566 Ci/mol]) at the time of injection. Eighteen serial dynamic PET images were acquired during the first 95 min after injection of each radioligand using the following image sequence: 4×15 s frames, 3×1 min frames, 3×2 min frames, 3×5 min frames, 3×10 min frames, and 2×20 min frames. Correct positioning of the head of the animal was closely monitored using a laser guide and was corrected by repositioning when necessary. PET scans were reconstructed using ramp-filtered backprojection in a 128×128 matrix, with a transaxial pixel size of 2×2 mm.

Input Function

To obtain the input function, blood samples were collected from a tibial artery every 5 s during the first 2 min and then collected with increasing time intervals of 1–5 min until the end of the PET study. This input function was corrected for metabolized radioligand activity. For this purpose, 2-mL arterial plasma samples were obtained at 5, 15, 30, 60, and 90 min after injection and were analyzed for tracer metabolism. Missing data points were obtained by interpolation based on a monoexponential function that described the disappearance of the percentage of nonmetabolized tracer from circulation. Calculations were repeated with a biexponential fit of the high-performance liquid chromatographic (HPLC) data but these calculations resulted in higher parameter variance. Thus, data are shown with the first solution only.

Tracer Metabolism

The extent of metabolism of (+)- ^{11}C -McN5652 and ^{11}C -DASB was determined using a published method (23) with minor modifications. In particular, in the column-switch HPLC procedure, we used a capture column packed with Oasis sorbent (Waters Associates, Milford, MA) and a Prodigy ODS-2 10- μm 4.6×250 mm analytic column (Phenomenex, Torrance, CA). For (+)- ^{11}C -McN5652 analysis, plasma (2 mL) was made 8 mol/L in urea to disrupt strong protein binding, and the HPLC solvent was 40% acetonitrile in 0.1 mol/L triethylamine acetate buffer, pH 4.1 (v/v) at a flow rate of 1.4 mL/min. For ^{11}C -DASB analysis, urea treatment of the plasma was unnecessary, and the HPLC solvent was 40% acetonitrile in 0.1 mol/L ammonium formate (v/v) at a flow rate of 3 mL/min.

Plasma Protein Binding

To determine protein binding, the radioligands were diluted in either plasma or saline. The solutions, without pH control, were added to Centrifree devices (YM-30, Amicon; Millipore, Bedford, MA) and centrifuged in an angle rotor at approximately 400g at room temperature. Radioactivity in samples of the original solutions, their filtrates, the filtrate collection cups, and filters was

determined. The ratio of radioactivity in the original solution and the filtrate, corrected for binding to the filtrate collection cup and filter, was used to estimate the percentage of ligand bound to plasma protein.

Image Processing

PET and MR images were converted to NetCDF (34)/MINC (http://www.bic.mni.mcgill.ca/software/minc/minc.html) format (24). For image coregistration, the AIR package was implemented (25,26). For image conversion, display, fusion, region drawing, and time–activity curve generation, a custom-made software running under Windows was developed in C++ and MatLab 5.3 (The Mathworks, Natick, MA). All PET data were corrected for attenuation, injected dose (ID), and radionuclide decay. For calculation of the 3-dimensional image transformation matrix, the PET images were summed over time. In the MRI volume data, outlines of the brain were determined manually and voxels outside the brain were removed by masking. The MRI scans were reoriented to match the PET slices during 3-dimensional registration. To derive volumetric time–activity curves, circular regions of interest (ROIs) of identical sizes were generated and displayed simultaneously on PET, MR, and fused images. The following brain regions were analyzed: cerebellum, thalamus, caudate, putamen, temporal cortex, frontal cortex, parietal cortex, occipital cortex, cingulate gyrus, midbrain, hypothalamus, and pons (Fig. 1). An exact delineation of the hypothalamus was not possible and this ROI included, in addition, the hypothalamus structures such as the most ventral parts of the thalami and probably the most rostral parts of the midbrain as well. Each ROI was comprised of a tissue volume of 0.75 mL (voxel size, $2 \times 2 \times 4.25$ mm; 44 voxels per ROI). Central structures such as the caudate or putamen were represented by the activity concentration of individual ROIs; cortical and cerebellar structures were represented by average activity concentrations of multiple ROIs. ROIs in the frontal cortex and parietal cortex were defined at the level of centrum semiovale. The ROIs of the cingulate gyrus were defined in the brain slice above this level. Tissue time–activity curves were expressed in units of nCi/mL/mCi (37 Bq/mL/37 MBq) ID.

Compartmental Modeling

The kinetics of the radioligand were described by models based on 1 or 2 tissue compartments, with or without inclusion of a regional cerebral blood volume term (BV). The mathematic details of these models have been reported (14). The most simple model consists of a single tissue compartment, and the distribution kinetics of the radioligand are described by 2 parameters: tissue uptake, $K_{1,2\text{par}}$, and release, $k_{2,2\text{par}}$. The more complex model consists of 2 tissue compartments (1 for specific binding and another for non-specific binding) and of a blood-pool component described by the regional cerebral blood volume ($BV_{5\text{par}}$). In this model, $K_{1,5\text{par}}$ and $k_{2,5\text{par}}$ describe uptake and release of the radioligand in the brain tissue, whereas $k_{3,5\text{par}}$ and $k_{4,5\text{par}}$ describe binding and release of the radioligand at the site of the SERT. Statistical tests corroborated the model that described radioligand kinetics by a single tissue compartment and 3 parameters: $BV_{3\text{par}}$ = blood volume, $K_{1,3\text{par}}$ = uptake of radioligand in brain tissue, and $k_{2,3\text{par}}$ = release of radioligand from brain tissue (3par in the subscript denotes the 3-parameter model). From this model, the total apparent distribution volume was calculated as $DV = K_{1,3\text{par}}/k_{2,3\text{par}}$ (14,27). Model parameters were estimated by the Marquardt algorithm (28), minimizing the sum of the squared differences between the measured and fitted tissue activity curves.

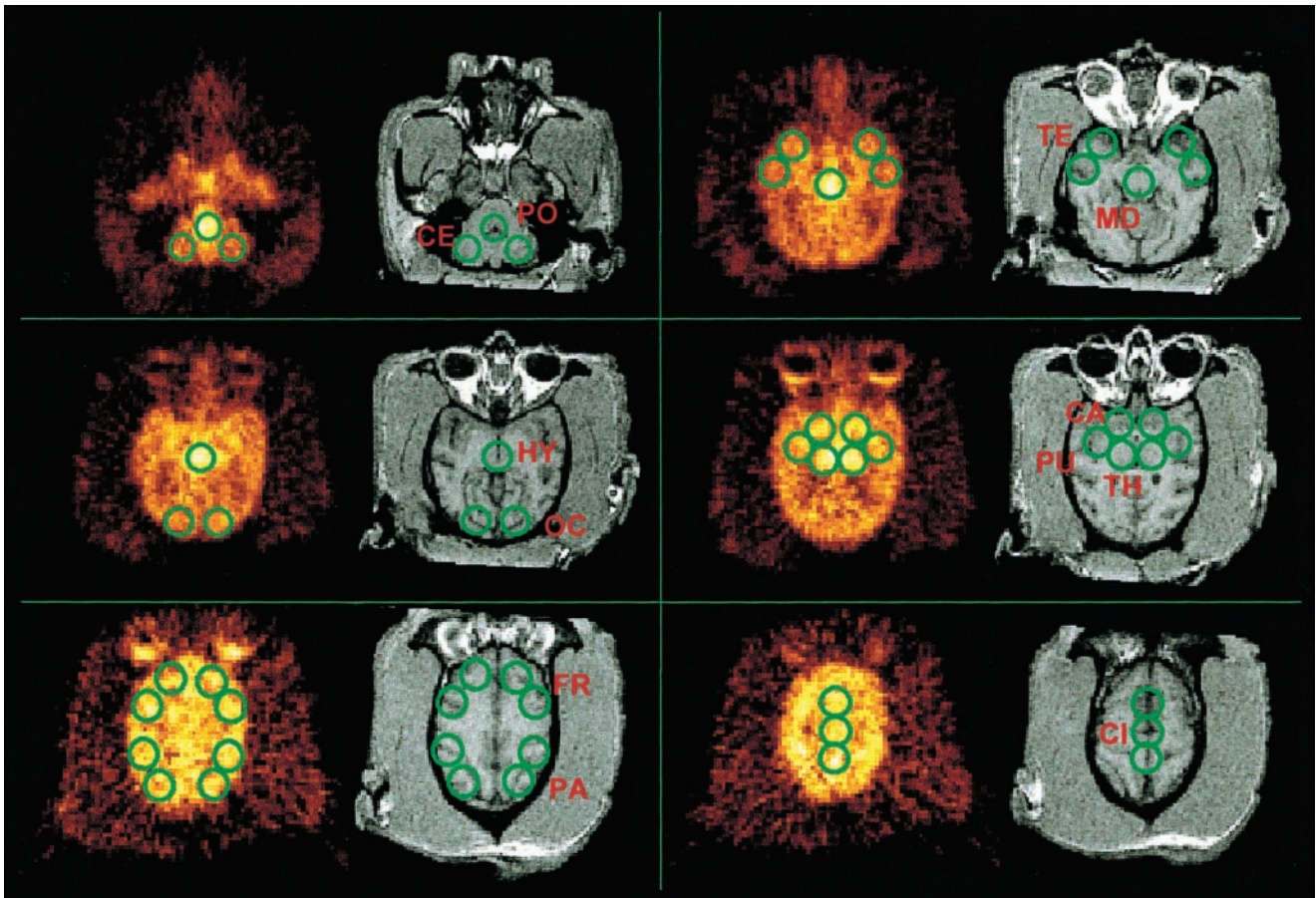


FIGURE 1. Registered PET ^{11}C -DASB and MR images of control baboon brain with superimposed ROIs used for derivation of time-activity curves. PO = pons; CE = cerebellum; TE = temporal cortex; MD = midbrain; HY = hypothalamus; OC = occipital cortex; CA = head of caudate; PU = putamen; TH = thalamus; FR = frontal cortex; PA = parietal cortex; CI = cingulate gyrus.

In Vitro Assays

Baboons were killed with an intravenous overdose of pentobarbital. The brains were immediately dissected on ice and the samples were stored at -70°C until further processing. Regional brain levels of 5-HT and 5-hydroxyindoleacetic acid (5-HIAA) and SERT binding densities were measured as described (29). Baboons killed for this study included the 3 that served as control animals for the neurochemical studies and the 1 that was lesioned with MDMA before PET imaging.

Quantitative Autoradiography

The saline-treated and the MDMA-treated baboons that had undergone PET studies were killed as described, and the brain was rapidly removed in a cold room (4°C), blotted, and immersed in isopentane packed in dry ice to ensure uniform freezing. The frozen brain parts were then stored in a -80°C freezer until sectioning. For SERT binding studies, methods described earlier were used (20).

Statistical Analysis

Regional tissue activities of (+)- ^{11}C -McN5652 and ^{11}C -DASB were determined for the time interval from 75 to 95 min and compared by linear correlation. The interdependence of DV of the 2 radioligands was also tested by linear correlation. Parameter variance was expressed by SD. Intrasubject reproducibility was measured by the coefficient of variation CV calculated from the SD

of triplicate measurements. The effect of prior MDMA lesioning or paroxetine pretreatment on regional tracer accumulation and compartmental parameters was evaluated by ANOVA, which was performed separately to compare saline versus MDMA treatment (lesioned vs. unlesioned) and saline versus paroxetine pretreatment (blocked vs. unblocked). The Bonferroni correction for multiple comparisons was performed to account for the number of ROIs. The probability of a null hypothesis was assessed both without and with Bonferroni correction for multiple comparisons (30). An ANOVA F value was calculated during parameter estimation for statistical testing of model order. Instability of the parameter estimator was assessed by the condition number of the parameter variance-covariance matrix (14,31). Compartmental parameter estimation and statistical testing of the parameter estimator were performed using the numeric software package MATLAB/Windows version 5.3 (The Mathworks). Conventional statistical tests were performed with the SPSS software package for Windows NT, version 10 (SPSS, Inc., Chicago, IL).

RESULTS

Time-Activity Curves

Accumulation and Distribution of (+)- ^{11}C -McN5652 and ^{11}C -DASB. After radioligand injection, regional brain activity of both radiotracers gradually increased, with highest

TABLE 1

Average Regional Tissue Radioactivity Measured 75–95 Minutes After Injection of (+)-¹¹C-McN5652 or ¹¹C-DASB

Radioligand*	Pons	MB	Hypo	Thalamus	Put	Cd	FC	PC	TC	CC	OC	Cereb
¹¹ C-McN5652												
Control	139 ± 9	144 ± 19	165 ± 21	144 ± 21	113 ± 7	105 ± 7	75 ± 12	85 ± 5	87 ± 10	83 ± 9	86 ± 9	84 ± 7
MDMA	100 ± 3 ^{†‡}	115 ± 3	117 ± 10 [†]	88 ± 12 [†]	70 ± 2 ^{†‡}	73 ± 7 [†]	51 ± 5 [†]	52 ± 3 ^{†‡}	63 ± 12 [†]	56 ± 5 [†]	50 ± 7 [†]	53 ± 3 ^{†‡}
Paroxetine	94 ± 24 [†]	99 ± 14 [†]	98 ± 21 [†]	106 ± 22	115 ± 28	105 ± 22	84 ± 12	92 ± 14	92 ± 10	85 ± 19	93 ± 16	86 ± 17
¹¹ C-DASB												
Control	188 ± 24	194 ± 31	229 ± 33	185 ± 33	122 ± 16	136 ± 26	59 ± 3	56 ± 7	72 ± 9	72 ± 14	56 ± 5	55 ± 9
MDMA	117 ± 17 [†]	124 ± 16 [†]	134 ± 29 [†]	86 ± 16 [†]	49 ± 10 ^{†‡}	62 ± 7 [†]	30 ± 2 ^{†‡}	29 ± 2 ^{†‡}	39 ± 9 [†]	36 ± 2 [†]	30 ± 3 ^{†‡}	30 ± 3 [†]
Paroxetine	56 ± 9 [†]	54 ± 9 [†]	54 ± 5 [†]	56 ± 3 [†]	55 ± 2 ^{†‡}	51 ± 5 ^{†‡}	49 ± 5 [†]	53 ± 3	57 ± 3 [†]	48 ± 3 [†]	50 ± 5	44 ± 5

*Each radioligand was tested 3 times in control baboon or different baboon lesioned previously with serotonergic neurotoxin MDMA.
[†]Designates significant difference from control (ANOVA without correction for multiple comparisons).
[‡]Designates significant difference from control (ANOVA with correction for multiple comparisons).
^{||}Designates significant difference from MDMA (ANOVA without correction for multiple comparisons).
 MB = midbrain; Hypo = hypothalamus; Put = putamen; Cd = caudate; FC = frontal cortex; PC = parietal cortex; TC = temporal cortex; CC = cingulate cortex; OC = occipital cortex; Cereb = cerebellum.
 Values represent mean ± SD (n = 3).

activity levels developing in the pons, midbrain, hypothalamus, striatum, and thalamus (Table 1; Fig. 2). As in previous studies (11), average regional brain tissue radioactivity measured 75–95 min after injection (TA_{75–95}) of (+)-¹¹C-McN5652 corresponded well with the distribution of the SERT in the baboon brain measured in vitro ($y = 0.0264x + 66$; $r = 0.946$), which, in turn, correspond well to the known distribution of the SERT in the human brain (32–34). There were also high correlations between the regional TA_{75–95} of (+)-¹¹C-McN5652 and 2 other serotonergic axonal markers, 5-HT ($y = 0.104x + 75$; $r = 0.862$) and 5-HIAA ($y = 0.0627x + 78$; $r = 0.926$). The same was true for ¹¹C-DASB: SERT ($y = 0.059x + 26$; $r = 0.969$), 5-HT ($y = 0.2235x + 43$; $r = 0.895$), and 5-HIAA ($y = 0.1284x + 53$; $r = 0.911$). There was an excellent correlation between the regional distribution of the 2 radioligands (DASB on MCN5652: $y = 2.087x - 109$; $r = 0.958$). In regions with higher SERT densities, TA_{75–95} was generally higher with ¹¹C-DASB than with (+)-¹¹C-McN5652. Conversely, in regions with lower SERT density (cerebral cortical regions, cerebellum), TA_{75–95} was generally lower with ¹¹C-DASB than with (+)-¹¹C-McN5652 (Table 1). Both ligands exhibited good test–retest reliability with interscan variance, estimated by the coefficient of variation, for (+)-¹¹C-McN5652 ranging from 6% to 17% and that of ¹¹C-DASB ranging from 7% to 19%, depending on brain region.

Effect of MDMA Treatment on (+)-¹¹C-McN5652 and ¹¹C-DASB Tissue Activity. Prior lesioning of 5-HT systems with neurotoxic doses of MDMA (to markedly reduce SERT density) resulted in significant reductions in regional activities of (+)-¹¹C-McN5652 and ¹¹C-DASB. When analyzed by ANOVA without Bonferroni correction for multiple comparisons, 11 of 12 regions examined with (+)-¹¹C-McN5652 and 12 of 12 regions with ¹¹C-DASB were significantly lower after MDMA (Table 1). After Bonferroni correction, 4 of 12 regions examined with each ligand achieved statistical significance ($P < 0.0042$). With (+)-¹¹C-McN5652, the regions were the pons, putamen, parietal

cortex, and cerebellum; with ¹¹C-DASB, the regions were frontal cortex, parietal cortex, occipital cortex, and putamen (Table 1). As in the saline-treated baboon, correlation analysis showed strong correlations between the imaging findings and the postmortem neurochemical findings in the MDMA-treated baboon. For (+)-¹¹C-McN5652, SERT ($y = 0.0432x + 50.72$; $r = 0.958$), 5-HT ($y = 0.0826x + 58.69$; $r = 0.863$), 5-HIAA ($y = 0.0736x + 56.47$; $r = 0.956$); and for ¹¹C-DASB, SERT ($y = 0.0684x + 25.88$; $r = 0.923$), 5-HT ($y = 0.1348x + 38.48$; $r = 0.879$), and 5-HIAA ($y = 0.1196x + 34.94$; $r = 0.969$).

Effect of Paroxetine on (+)-¹¹C-McN5652 and ¹¹C-DASB Tissue Activity. Pretreatment with paroxetine to reduce SERT availability markedly altered the rate of uptake of both radioligands, with more rapid early peaks than those seen under baseline conditions or after MDMA treatment (Fig. 2). Indeed, the average brain tissue activity measured during the first 5 min was increased by 40% for (+)-¹¹C-McN5652 and by 106% for ¹¹C-DASB. Pretreatment with paroxetine also inhibited the metabolism of both radioligands. In light of these effects of paroxetine on ligand kinetics and metabolism, comparisons between average regional tissue radioactivity measured 75–95 min after ligand injection (TA_{75–95}) under baseline conditions and after pretreatment with paroxetine must be interpreted with caution (i.e., differences may not fully or solely reflect displacement from specific binding sites).

With these potential caveats in mind, pretreatment with paroxetine led to reductions in TA_{75–95} of both radioligands compared with the baseline condition, with the extent of reduction varying across regions and depending on the ligand. As before, the statistical significance of the observed differences depended on whether the ANOVA analysis included a correction for multiple comparisons. For example, ANOVA without the Bonferroni correction showed significant reductions in TA_{75–95} of (+)-¹¹C-McN5652 in some (pons, midbrain, hypothalamus) but not all (thalamus, putamen, and caudate) regions with higher SERT density.

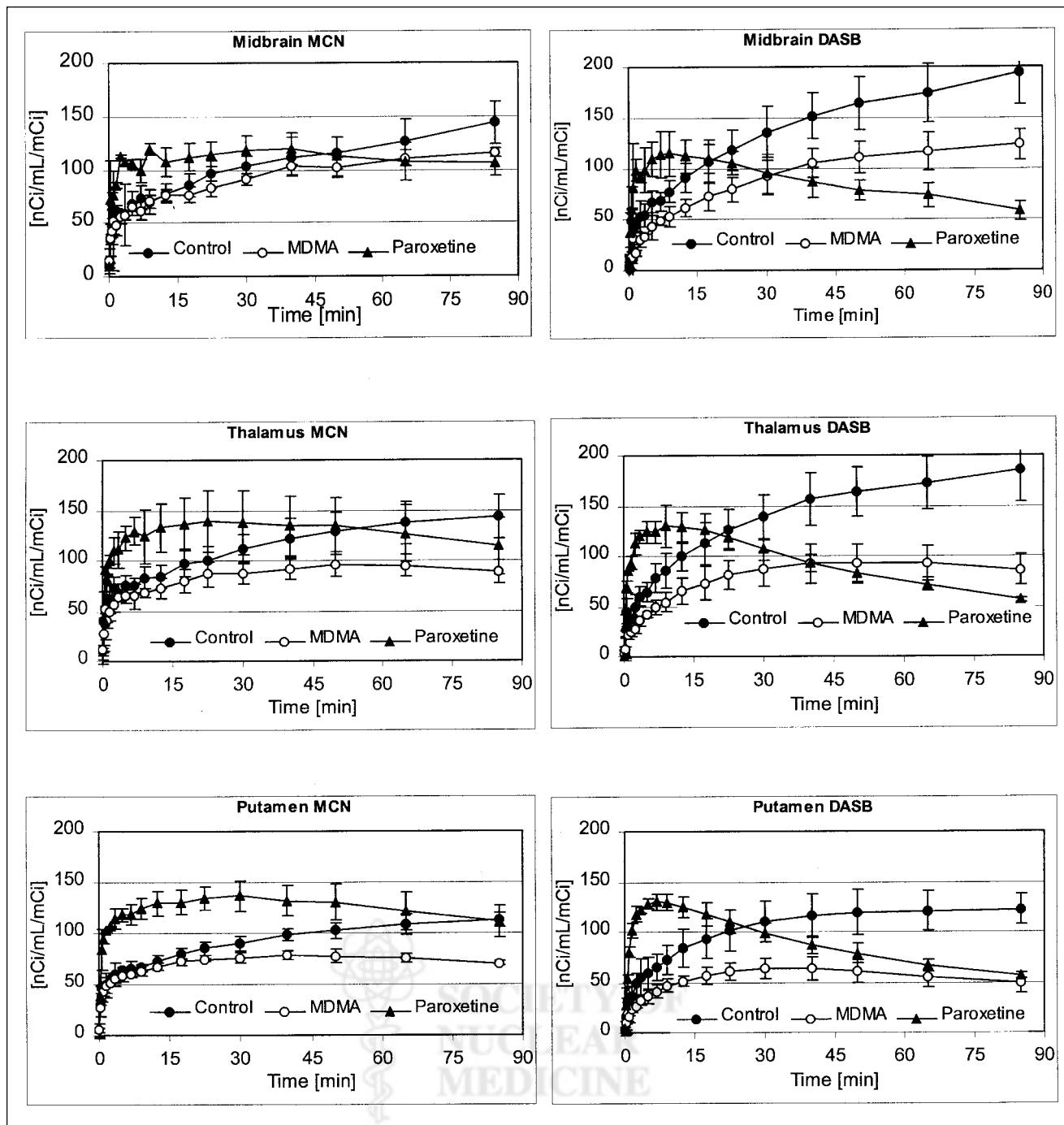


FIGURE 2. Time-activity curves obtained with (+)-¹¹C-McN5652 (left) and ¹¹C-DASB (right) in various ROIs. Shown are results under baseline conditions and after MDMA treatment and paroxetine pretreatment. Data are expressed in units of nCi/mL/mCi (37 Bq/mL/37 MBq) ID. Measured data are displayed with circles; curves fitted on basis of 3-parameter, 1-tissue compartment model are displayed with lines. Both radioligands show decreased binding in MDMA-treated animal compared with control animal. With both radioligands, paroxetine increased amount of radioactivity reaching brain, measured as time integral of unmetabolized radioligand concentration in arterial plasma. (Continued on page 684.)

Indeed, in these 2 brain regions (putamen and caudate), as well as in regions with low SERT density (cortical regions and cerebellum), TA₇₅₋₉₅ of ¹¹C-(+)-McN5652 after paroxetine pretreatment was actually higher than that after MDMA, possibly secondary to the effects of paroxetine on

¹¹C-(+)-McN5652 metabolism and uptake in the brain. After posthoc correction, paroxetine pretreatment produced no significant effects on (+)-¹¹C-McN5652 binding, probably caused by the high variability of the paroxetine data (Table 1).

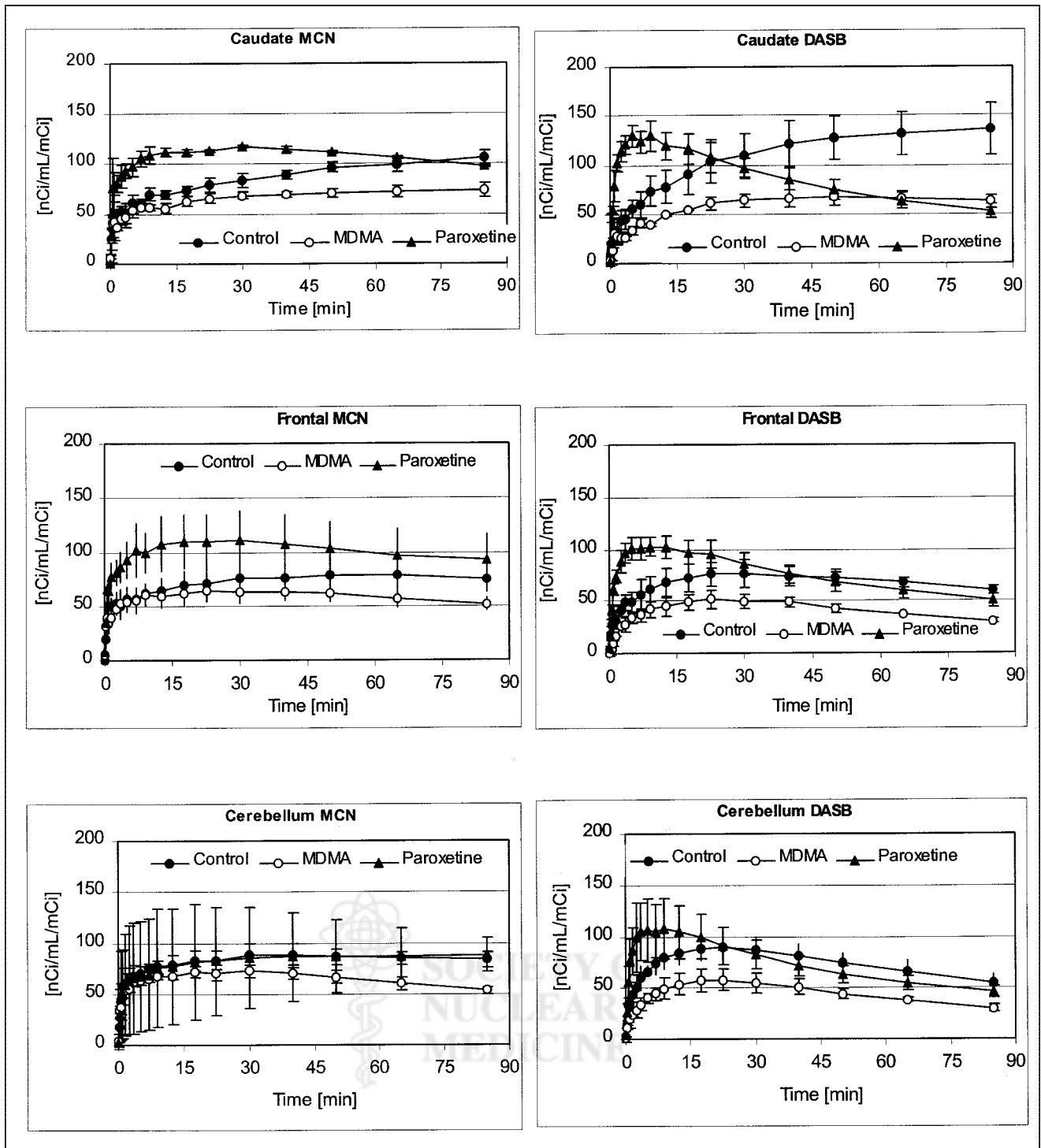


FIGURE 2. (See legend on page 683.)

For ^{11}C -DASB, ANOVA without correction for multiple comparisons showed that paroxetine pretreatment led to significant reductions in TA_{75-95} in the 9 of 12 regions examined (Table 1). With the Bonferroni correction, 5 of 12 regions remained significantly different. Typically, reductions in ^{11}C -DASB activity after paroxetine were greater than those after MDMA (Table 1). Exceptions were all of the cortical regions analyzed and the cerebellum (Table 1).

There appeared to be a floor effect in the extent to which paroxetine could decrease the activity of both radioligands. Thus, for (+)- ^{11}C -McN5652, no average values were observed below 3,145 Bq/mL tissue/37 MBq (85 nCi/mL tissue/mCi) ID (Table 1), in contrast to levels of approximately 1,850 Bq/mL tissue/37 MBq (50 nCi/mL tissue/mCi) ID in several brain regions after MDMA treatment (Table 1). Similarly, for ^{11}C -DASB, no average values were

observed below 1,628 Bq/mL tissue/37 MBq (44 nCi/mL tissue/mCi) ID, in contrast to levels of approximately 1,110 Bq/mL tissue/37 MBq ID (approximately 30 nCi/mL tissue/mCi) in several brain regions of the MDMA-treated baboon (Table 1).

Variability in tissue radioactivity 75–95 min after injection (TA_{75-95}) of (+)- ^{11}C -McN5652 after paroxetine treatment was much greater than that seen after neurotoxic injury with MDMA (Table 1), possibly as a result of paroxetine's effects on ligand metabolism and kinetics. In addition, 1 of the 3 studies with paroxetine yielded absolute values that, though suggesting SERT blockade, were higher than those obtained in the 2 other studies and contributed to the high variance. In contrast, variability in TA_{75-95} of ^{11}C -DASB after paroxetine was similar or smaller than that after treatment with MDMA.

Relation of Tissue Radioactivity to In Vitro Measures of 5-HT Axonal Markers. As anticipated on the basis of prior findings (11), compared with average normal values obtained in 3 control baboons, in vitro parameters of 5-HT axonal markers in the MDMA-treated animal were markedly reduced. Decreases of 5-HT axonal markers were region dependent, with the most severe reductions evident in cerebral cortical regions, thalamus, putamen, and caudate (Fig. 3A–C). Quantitative autoradiographic studies with 3H -citalopram provided additional evidence of profound MDMA-induced 5-HT neurotoxicity. A coronal section of the control baboon brain (Fig. 4) revealed intense radioligand binding in the basal ganglia with less binding in the temporal cortex, cingulate gyrus, and dorsal neocortex. As is evident from Figure 4, MDMA treatment reduced ligand binding in all of these brain regions. Similarly, autoradiography at the level of the cerebellum and brain stem (Fig. 5) showed high SERT density in the raphe nuclei, with somewhat less binding in the ventral and rostral brain stem. Importantly, 3H -citalopram binding in the folia cerebelli (Fig. 5) of the control baboon confirmed that the cerebellum is not devoid of SERT sites (32–36). The same brain section

of the MDMA-treated animal showed decreased ligand binding in most of these areas (including the cerebellum), although small islands of high activity remained in the dorsal brain stem (dorsal raphe) (Fig. 5).

Notably, both PET radioligands underestimated the extent of 5-HT axonal marker depletion produced by MDMA (Fig. 3), with (+)- ^{11}C -McN5652 showing reductions of approximately 30% in most regions up to a maximum of 42% in the occipital cortex (Table 1). ^{11}C -DASB was slightly better in this regard, generally showing reductions of 40%–45%, with the greatest reduction of 60% seen in the putamen (Table 1). These underestimations may be, to a large degree, attributable to nonspecific binding of the radioligands.

Plasma Analysis and Protein Binding of Radioligands

The metabolism of both radioligands was relatively rapid. The estimated biologic half-life ($t_{1/2}$) of (+)- ^{11}C -McN5652 was 42 min and that of ^{11}C -DASB was 30 min. Prior MDMA treatment produced no significant effect on the rate of tracer metabolism. In contrast, pretreatment with paroxetine reduced the rate of metabolism of both radioligands. After paroxetine, the plasma $t_{1/2}$ of (+)- ^{11}C -McN5652 was prolonged to 75 min (79% increase), and that of ^{11}C -DASB was increased to 38 min (27% increase).

The metabolism of both ligands led to very polar metabolites and 1 or more lipophilic metabolites. The polar metabolites failed to bind to the Oasis capture column. The lipophilic metabolites and parent compounds were removed from the plasma by the Oasis sorbent in the capture column and were eluted by the analytic solvent at the time of the column switch. Thirty minutes after injection of the ligands, highly polar products accounted for 19% of the total ^{11}C -DASB radioactivity and 7% of the total (+)- ^{11}C -McN5652 radioactivity.

Determination of plasma protein binding using Centrifree devices suffered from binding artifacts for (+)- ^{11}C -McN5652 and ^{11}C -DASB. These artifacts were less signif-

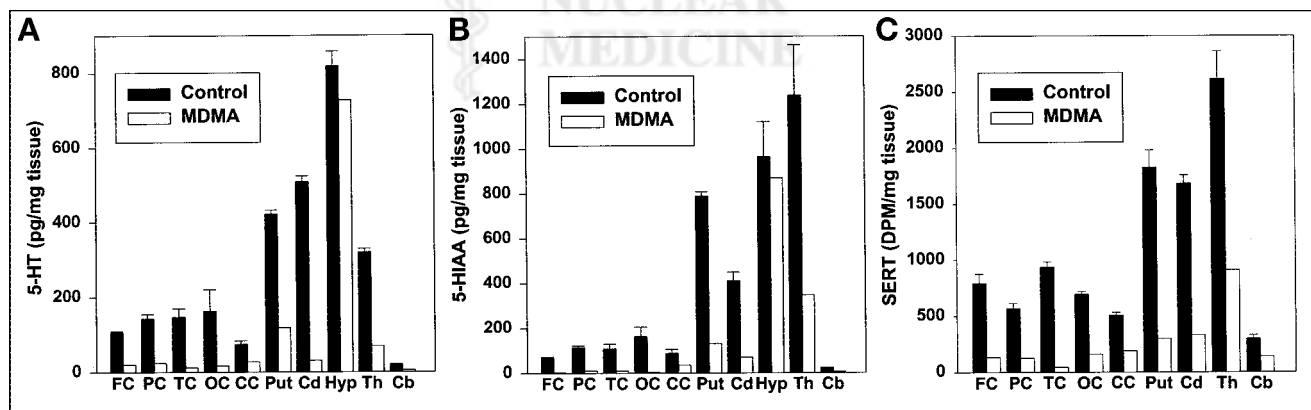


FIGURE 3. Effect of prior lesioning of brain 5-HT neurons with MDMA on regional brain 5-HT (A), 5-HIAA (B), and SERT (C) concentrations. FC = frontal cortex; PC = parietal cortex; TC = temporal cortex; OC = occipital cortex; CC = cingulate cortex; Put = putamen; Cd = caudate; Hyp = hypothalamus; Th = thalamus; Cb = cerebellum; DPM = disintegrations per minute.

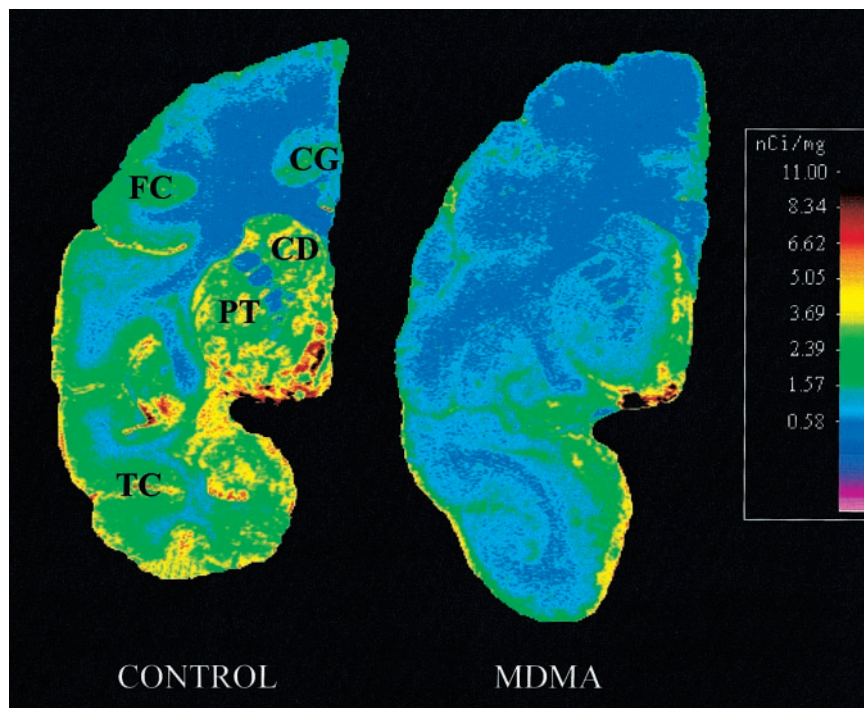


FIGURE 4. Autoradiography of SERT in baboon brain: coronal section of frontal/temporal/parietal cortex and basal ganglia. In control animal, intense ligand binding is seen in basal ganglia (CD = caudate; PT = putamen). Less binding is seen in temporal cortex (TC), cingulate gyrus (CG), and frontal cortex (FC). MDMA treatment reduced ligand binding in most represented brain structures.

inant in the presence of plasma because the protein binding competed successfully with the components of the filtration device. By measuring the radioactivity associated with each component of the system, 89% of ^{11}C -DASB and 99% of (+)- ^{11}C -McN5652 were determined to be bound to plasma proteins.

Kinetic Modeling

(+)- ^{11}C -McN5652. The statistically best curve fit was obtained with a 3-parameter, 1-tissue compartment model

(37). ANOVA of the sums of squared residuals resulted in an average F value of 16.2 ($P < 0.005$), consistent with an improved curve fit with the 3-parameter model compared with the 2-parameter model. The 4-parameter model was statistically inferior to the 3-parameter model ($F = -8.97$; $P < 0.005$), whereas the 5-parameter model was statistically indistinguishable from the 3-parameter model (average $F = 2.54$; not significant). The average condition number of the 3-parameter model was 3.90 ± 0.71 , only 1.08 times higher

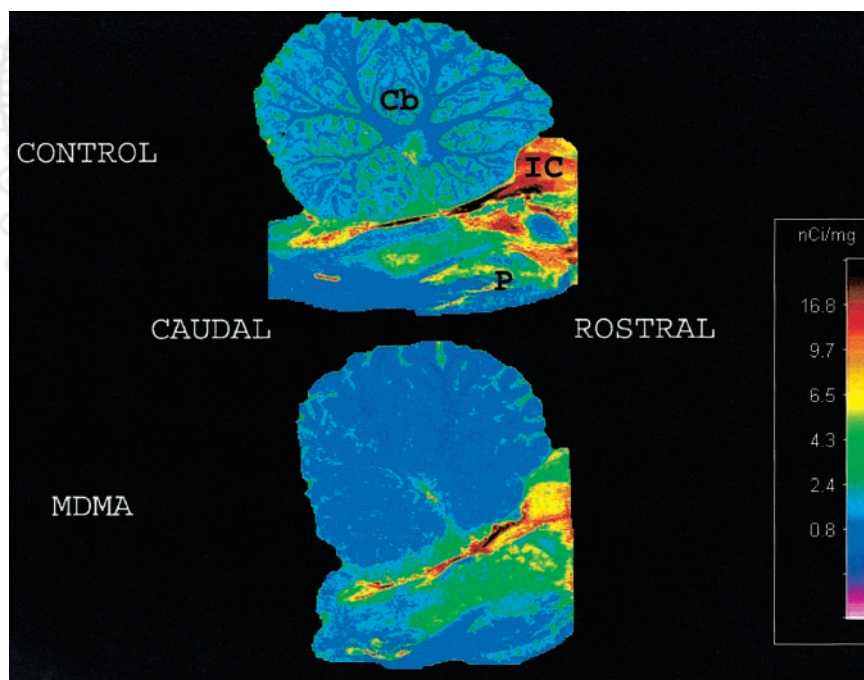


FIGURE 5. Autoradiography of SERT in baboon brain: sagittal section at level of cerebellum and brain stem. In control animal (top), there is high radioligand binding in dorsal brain stem. Less intense, but still significant, binding is seen in ventral and rostral brain stem. There is low but obvious binding in folia cerebelli. In MDMA-treated animal (bottom), binding is decreased in most of these areas, although small islands of high activity remain in dorsal brain stem. In MDMA-treated baboon, radioligand binding is almost completely absent in cerebellum. ROSTRAL and CAUDAL = axes of brain stem; Cb = cerebellum; IC = inferior colliculus; P = pons.

than the average condition number of the 2-parameter model. On the other hand, the condition number of the 4-parameter model was 10 times higher than the condition number of the 3-parameter model. The condition number of the 5-parameter model was 13 times higher than the condition number of the 3-parameter model. These increments indicated deterioration of the conditioning of the parameter estimator with increasingly complex models (e.g., the 2-tissue compartment, 4- and the 5- parameter models). On the basis of the results of these analyses, the 3-parameter model was chosen for derivation of the *DV* of (+)-¹¹C-McN5652.

¹¹C-DASB. The 3-parameter model produced statistically insignificant improvement compared with the 2-parameter model (average *F* = 3.36; not significant). The condition number of the 3-parameter model was 4.4, or 20% greater than the condition number of the 2-parameter model. More complex models with 2 tissue compartments and 4 or 5 parameters resulted in statistically insignificant ANOVA *F* values. These complex models were associated with deterioration of model conditioning (e.g., a 13- to 14-fold increase in the condition number of the parameter variance-covariance matrix). Because the 2-parameter and 3-parameter models (*BV*, *K*₁, *k*₂) resulted in statistically comparable conditioning, the 3-parameter model was used for description of the kinetics of ¹¹C-DASB to facilitate comparison with ¹¹C-McN5652, the kinetics of which were described with a 3-parameter model.

Regional Brain *DVs* of (+)-¹¹C-McN5652 and ¹¹C-DASB

Like regional radioactivity tissue accumulation (Table 1), *DVs* of (+)-¹¹C-McN5652 and ¹¹C-DASB were highest in brain regions known to contain high SERT density (Table 2). There was an excellent correlation between *DVs* of the 2 radioligands in the various brain regions examined (*r* = 0.92). As seen with TA₇₅₋₉₅ levels, *DVs* of ¹¹C-DASB were higher than those of (+)-¹¹C-McN5652 in brain regions known to have high SERT density (e.g., midbrain), while brain regions with lower SERT density showed higher *DVs* using (+)-¹¹C-McN5652 versus ¹¹C-DASB. With both ra-

dioligands, there was increased variability of *DV* values in brain regions known to contain high SERT density, a phenomenon more pronounced with ¹¹C-DASB than with (+)-¹¹C-McN5652 (Table 2).

Effect of MDMA Treatment on Regional *DVs*

ANOVA without correction for multiple comparisons showed that the *DV* of (+)-¹¹C-McN5652 in the MDMA-treated baboon was reduced in 12 of 12 brain regions examined (Table 2). After Bonferroni correction, 11 of 12 regions remained significantly different for (+)-¹¹C-McN5652 (Table 2).

For ¹¹C-DASB, ANOVA without the Bonferroni correction showed that 8 of 12 regions had significantly lower *DVs* compared with the control (Table 2). With the Bonferroni correction, 1 of 12 regions remained significantly different for ¹¹C-DASB. The higher parameter variance of the *DV* of ¹¹C-DASB was caused, in part, by the slightly more unstable compartmental model used for ¹¹C-DASB and, in part, by the higher variance in tissue activity (Table 2).

The effect of MDMA on regional *DV* values of the 2 ligands was largely attributable to radioligand retention rather than altered uptake. This is evidenced by the fact that uptake, expressed by *K*₁ of the compartmental model, did not differ significantly after MDMA for either (+)-¹¹C-McN5652 or ¹¹C-DASB in any brain region (Table 3). In contrast, after MDMA, the *k*₂ of (+)-¹¹C-McN5652 and ¹¹C-DASB increased across almost all brain regions (Table 4). Thus, changes in *k*₂ far outweigh changes of *K*₁. Interestingly, the *K*₁ of ¹¹C-DASB was, on average, 22% higher than the *K*₁ of (+)-¹¹C-McN5652, consistent with a higher uptake of ¹¹C-DASB into brain tissue.

Effect of Paroxetine Pretreatment

The amount of radioligand reaching the brain measured as the time integral of the unmetabolized radioligand concentration in arterial plasma was increased after paroxetine by an average of 25% for (+)-¹¹C-McN5652 and 44% for ¹¹C-DASB. Paroxetine treatment had a negligible effect on

TABLE 2
Regional *DV* Values After Injection of (+)-¹¹C-McN5652 or ¹¹C-DASB

Radioligand*	Pons	MB	Hypo	Thalamus	Put	Cd	FC	PC	TC	CC	OC	Cereb
¹¹ C-McN5652												
Control	29.4 ± 1.4	40.2 ± 2.7	46.1 ± 2.6	33.4 ± 1.2	23.6 ± 1.3	22.0 ± 1.4	12.9 ± 0.3	14.4 ± 0.5	15.5 ± 0.2	14.9 ± 0.5	14.3 ± 0.2	13.7 ± 0.3
MDMA	17.4 ± 1.2††	22.5 ± 2.5†	21.2 ± 2.4††	14.4 ± 0.6††	11.2 ± 0.7††	11.8 ± 0.9††	8.2 ± 0.6††	8.6 ± 0.4††	10.0 ± 0.8††	9.2 ± 0.3††	8.4 ± 0.4††	8.7 ± 0.4††
Paroxetine	14.8 ± 3.2†	15.3 ± 2.7††	15.3 ± 2.8†	16.9 ± 3.3†	18.3 ± 3.6	16.7 ± 3.1	13.2 ± 2.2	14.3 ± 2.4	15.1 ± 1.8	13.5 ± 2.5	14.3 ± 2.4	13.0 ± 2.3
¹¹ C-DASB												
Control	46.2 ± 11.1	71.3 ± 14.8	79.8 ± 11.2	45.5 ± 4.5	22.2 ± 3.3	27.5 ± 2.7	9.8 ± 1.3	9.2 ± 1.0	11.6 ± 1.4	11.5 ± 1.4	9.0 ± 0.9	9.2 ± 0.7
MDMA	26.5 ± 2.7	31.3 ± 1.4	31.3 ± 5.6†	15.9 ± 1††	8.9 ± 0.9†	11.5 ± 0.9†	6.1 ± 0.2	5.9 ± 0.3†	7.2 ± 0.7	6.9 ± 0.3†	6.0 ± 0.3†	6.3 ± 0.4†
Paroxetine	7.7 ± 0.8††	7.9 ± 0.8††	8 ± 0.8††	8.3 ± 0.6††	7.9 ± 0.6†	7.6 ± 0.7††	6.9 ± 0.7	7.3 ± 0.5	7.4 ± 0.6	7.1 ± 0.6†	7.3 ± 0.5	6.9 ± 0.7

*Each radioligand was tested 3 times in control baboon or different baboon lesioned previously with serotonergic neurotoxin MDMA.

†Designates significant difference from control (ANOVA without correction for multiple comparisons).

††Designates significant difference from control (ANOVA with correction for multiple comparisons).

‡Designates significant difference from MDMA (ANOVA without correction for multiple comparisons).

MB = midbrain; Hypo = hypothalamus; Put = putamen; Cd = caudate; FC = frontal cortex; PC = parietal cortex; TC = temporal cortex; CC = cingulate cortex; OC = occipital cortex; Cereb = cerebellum.

Values represent mean ± SD (*n* = 3).

TABLE 3
Regional K_1 Values After Injection of (+)- ^{11}C -McN5652 or ^{11}C -DASB

Radioligand*	Pons	MB	Hypo	Thalamus	Put	Cd	FC	PC	TC	CC	OC	Cereb
^{11}C -McN5652												
Control	0.29 ± 0.03	0.24 ± 0.02	0.30 ± 0.04	0.28 ± 0.01	0.24 ± 0.02	0.22 ± 0.02	0.23 ± 0.02	0.27 ± 0.02	0.23 ± 0.01	0.23 ± 0.01	0.30 ± 0.02	0.29 ± 0.02
MDMA	0.26 ± 0.04	0.25 ± 0.02	0.27 ± 0.02	0.28 ± 0.02	0.26 ± 0.02	0.21 ± 0.02	0.25 ± 0.05	0.31 ± 0.03	0.23 ± 0.02	0.29 ± 0.02	0.35 ± 0.03	0.30 ± 0.01
Paroxetine	0.27 ± 0.04	0.25 ± 0.05	0.30 ± 0.06	0.30 ± 0.07	0.32 ± 0.10	0.29 ± 0.08	0.24 ± 0.03	0.28 ± 0.04	0.21 ± 0.04	0.25 ± 0.06	0.30 ± 0.06	0.29 ± 0.05
^{11}C -DASB												
Control	0.35 ± 0.02	0.30 ± 0.04	0.36 ± 0.05	0.33 ± 0.04	0.29 ± 0.01	0.27 ± 0.02	0.26 ± 0.03	0.31 ± 0.05	0.27 ± 0.04	0.27 ± 0.04	0.34 ± 0.03	0.37 ± 0.06
MDMA	0.30 ± 0.05	0.28 ± 0.02	0.32 ± 0.04	0.31 ± 0.05	0.28 ± 0.02	0.24 ± 0.02	0.27 ± 0.06	0.33 ± 0.06	0.24 ± 0.02	0.30 ± 0.05	0.37 ± 0.05	0.34 ± 0.06
Paroxetine	0.39 ± 0.05	0.36 ± 0.05	0.43 ± 0.08	0.42 ± 0.03	0.46 ± 0.06†	0.46 ± 0.06†	0.35 ± 0.05	0.39 ± 0.05	0.27 ± 0.02	0.37 ± 0.03	0.42 ± 0.05	0.47 ± 0.06

*Each radioligand was tested 3 times in control baboon or different baboon lesioned previously with serotonergic neurotoxin MDMA.

†Designates significant difference from control (ANOVA without correction for multiple comparisons).

MB = midbrain; Hypo = hypothalamus; Put = putamen; Cd = caudate; FC = frontal cortex; PC = parietal cortex; TC = temporal cortex; CC = cingulate cortex; OC = occipital cortex; Cereb = cerebellum.

Values represent mean ± SD ($n = 3$).

the first-pass uptake of (+)- ^{11}C -McN5652, with an average increase of the K_1 value of only 6% (Table 3). Thus, the increased net uptake of (+)- ^{11}C -McN5652 during the first 5 min in the paroxetine-pretreated animal was attributable mainly to the higher amount of radioligand reaching the brain through the arterial circulation, probably secondary to less peripheral binding and the slower rate of (+)- ^{11}C -McN5652 metabolism in the presence of paroxetine. In contrast to (+)- ^{11}C -McN5652, the first-pass uptake of ^{11}C -DASB appeared to be affected by paroxetine because the average K_1 value of this radioligand increased, on average, by 30% in the presence of paroxetine (Table 3), contributing significantly to the effect of a 44% higher influx of unmetabolized ligand into the brain. The basis for the change of K_1 of ^{11}C -DASB after paroxetine treatment is unknown.

Table 2 illustrates the effect of paroxetine pretreatment on the DVs of (+)- ^{11}C -McN5652 and ^{11}C -DASB. Paroxetine pretreatment led to reductions in DVs of (+)- ^{11}C -McN5652 in some brain regions known to contain high levels of the SERT (pons, midbrain, hypothalamus, and thalamus). As with the TA_{75-95} data, there appeared to be a floor value beyond which paroxetine failed to displace (+)- ^{11}C -McN5652. In particular, paroxetine pretreatment failed

to reduce DVs of (+)- ^{11}C -McN5652 below a value of 13 in any region, in contrast to DVs as low as 8.2 (frontal cortex) and 8.4 (occipital cortex) after MDMA (Table 2). This was less evident for ^{11}C -DASB, although possibly still apparent in some regions (e.g., parietal cortex, 7.3 after paroxetine vs. 5.9 after MDMA; nonsignificant difference).

Compared with control values (ANOVA without posthoc correction), DVs after paroxetine pretreatment were significantly different in 4 of 12 regions with (+)- ^{11}C -McN5652 (pons, midbrain, hypothalamus, and thalamus) and in 7 of 12 regions with ^{11}C -DASB (same regions as (+)- ^{11}C -McN5652 plus caudate, putamen, and cingulate cortex). After Bonferroni correction, paroxetine pretreatment produced significant effects on 1 of 12 regions with (+)- ^{11}C -McN5652 and 3 of 12 regions with ^{11}C -DASB (hypothalamus, thalamus, and caudate).

Comparison with In Vitro Data

Modeling of the raw data led to some improvements in the estimations of SERT reductions produced by MDMA for both ligands, although PET data still underestimated the extent of the reductions in most brain regions. For example, DV values for (+)- ^{11}C -McN5652 were reduced by 53% (putamen) and 46% (caudate) in the MDMA-treated baboon

TABLE 4
Regional k_2 Values After Injection of (+)- ^{11}C -McN5652 or ^{11}C -DASB

Radioligand*	Pons	MB	Hypo	Thalamus	Put	Cd	FC	PC	TC	CC	OC	Cereb
^{11}C -McN5652												
Control	0.10 ± 0.00	0.06 ± 0.00	0.07 ± 0.01	0.08 ± 0.01	0.10 ± 0.00	0.10 ± 0.02	0.18 ± 0.01	0.19 ± 0.01	0.15 ± 0.01	0.15 ± 0.01	0.21 ± 0.02	0.21 ± 0.02
MDMA	0.15 ± 0.04†	0.11 ± 0.03†	0.13 ± 0.02†	0.19 ± 0.01†	0.24 ± 0.02†	0.18 ± 0.02†	0.30 ± 0.03†	0.36 ± 0.03†	0.23 ± 0.01†	0.32 ± 0.03†	0.42 ± 0.02†	0.35 ± 0.03†
Paroxetine	0.19 ± 0.04†	0.17 ± 0.02†	0.20 ± 0.03†	0.18 ± 0.02†	0.18 ± 0.01†	0.17 ± 0.01†	0.18 ± 0.03†	0.20 ± 0.03†	0.14 ± 0.01†	0.19 ± 0.02†	0.21 ± 0.02†	0.23 ± 0.03†
^{11}C -DASB												
Control	0.08 ± 0.03	0.05 ± 0.02	0.05 ± 0.01	0.07 ± 0.02	0.13 ± 0.03	0.10 ± 0.01	0.28 ± 0.07	0.34 ± 0.04	0.24 ± 0.03	0.24 ± 0.05	0.38 ± 0.06	0.40 ± 0.04
MDMA	0.11 ± 0.02	0.09 ± 0.00†	0.11 ± 0.02†	0.20 ± 0.00†	0.31 ± 0.03†	0.22 ± 0.02†	0.45 ± 0.09	0.56 ± 0.07	0.34 ± 0.04†	0.43 ± 0.06†	0.61 ± 0.03†	0.53 ± 0.05
Paroxetine	0.51 ± 0.03†	0.45 ± 0.02†	0.54 ± 0.02†	0.52 ± 0.03†	0.59 ± 0.06†	0.61 ± 0.06†	0.51 ± 0.05	0.54 ± 0.05	0.37 ± 0.03	0.52 ± 0.04†	0.58 ± 0.06	0.68 ± 0.04†

*Each radioligand was tested 3 times in control baboon or different baboon lesioned previously with serotonergic neurotoxin MDMA.

†Designates significant difference from control (ANOVA without correction for multiple comparisons).

‡Designates significant difference from control (ANOVA with correction for multiple comparisons).

MB = midbrain; Hypo = hypothalamus; Put = putamen; Cd = caudate; FC = frontal cortex; PC = parietal cortex; TC = temporal cortex; CC = cingulate cortex; OC = occipital cortex; Cereb = cerebellum.

Values represent $k_2 \times 10$ (mean ± SD [$n = 3$]).

as opposed to in vitro reductions of 72% and 94%, respectively, in the same regions. Reductions of DVs of (+)- ^{11}C -McN5652 in most cortical regions were roughly 40% compared with approximately 80% seen in vitro. For ^{11}C -DASB, DV reductions in the MDMA-treated baboon were slightly greater in subcortical regions than those seen with (+)- ^{11}C -McN5652 (e.g., 65% reduction in the thalamus vs. 57% using (+)- ^{11}C -McN5652, but slightly lower in cortical regions (e.g., 33% in occipital cortex vs. 41% using (+)- ^{11}C -McN5652).

DISCUSSION

Results from these studies indicate that (+)- ^{11}C -McN5652 and ^{11}C -DASB are suitable PET ligands for imaging of the SERT in nonhuman primates. Regional brain tissue activities and DVs of both radiotracers corresponded well to the known distribution of the SERT. Further, after treatment with the serotonergic neurotoxin MDMA, binding of both ligands decreased significantly, as would be anticipated in the setting of reduced SERT density. Reductions of in vitro measures of brain 5-HT axonal markers, measured in the same MDMA-treated baboon that had undergone PET imaging, corresponded well with reduced binding of both PET ligands, although PET imaging with both radioligands tended to underestimate the extent of 5-HT axonal loss. Pretreatment with the selective 5-HT reuptake inhibitor paroxetine also led to reductions in ligand binding, but the effects of paroxetine have to be interpreted with caution because of its effects on ligand metabolism and kinetics. Collectively, these results suggest that (+)- ^{11}C -McN5652 and ^{11}C -DASB are useful and reliable for measuring the SERT in nonhuman primates and for detecting MDMA-induced 5-HT neurotoxicity.

Despite numerous similarities between (+)- ^{11}C -McN5652 and ^{11}C -DASB, there were also some differences. For example, with ^{11}C -DASB, there was greater contrast than with (+)- ^{11}C -McN5652 between brain regions containing higher concentrations of the SERT (e.g., thalamus, midbrain) and brain regions with lower concentrations of the SERT (e.g., cerebral cortex, cerebellum). This difference between ^{11}C -DASB and (+)- ^{11}C -McN5652 may be due to the higher uptake of ^{11}C -DASB and to its faster apparent washout rate from binding sites. The faster apparent washout rate of ^{11}C -DASB may, in turn, be related to its more rapid metabolism in the periphery and to the fact that ^{11}C -DASB binds more weakly to plasma proteins than (+)- ^{11}C -McN5652. Despite these apparent advantages of ^{11}C -DASB over (+)- ^{11}C -McN5652, it is clear that under some experimental conditions (e.g., detecting MDMA neurotoxicity), the performance of the 2 ligands is comparable (Tables 1 and 2). Indeed, because of a lower binding variability at baseline, (+)- ^{11}C -McN5652 did slightly better than ^{11}C -DASB in detecting MDMA neurotoxicity (Tables 1 and 2). On the other hand, ^{11}C -DASB proved better than (+)- ^{11}C -McN5652 in the assessment of the effects of paroxetine. These differ-

ences between the 2 ligands suggest that choice of the optimal SERT ligand may be dependent on the study design and the question being investigated.

There is no consensus on the optimal method for defining nonspecific binding of (+)- ^{11}C -McN5652. Indeed, the optimal method for defining nonspecific binding of ^{11}C -DASB also remains to be determined. For ^{11}C -McN5652, we previously have used its inactive enantiomer, (-)- ^{11}C -McN5652, to define nonspecific binding, reasoning that similarity in kinetics and its poor affinity for the SERT made it ideal for this purpose. In this study, we explored the possibility that the selective 5-HT reuptake inhibitor paroxetine could be used to define nonspecific binding. However, results from studies with paroxetine were not straightforward. In particular, paroxetine decreased the rate at which unmetabolized tracer disappeared from the circulation and increased the amount of radioligand reaching the brain (measured as the time integral of the unmetabolized radioligand concentration in arterial plasma). In addition, paroxetine substantially increased the K_1 of ^{11}C -DASB and, for both ligands, there appeared to be a point beyond which paroxetine failed to block radioligand binding. This apparent floor effect was particularly evident with ^{11}C -McN5652 in cortical regions and the cerebellum, where binding after neurotoxic injury with MDMA was consistently lower than binding after paroxetine (Table 1). A similar effect was evident with ^{11}C -DASB when considering the TA_{75-95} data (Table 1). Thus, use of paroxetine to define nonspecific binding of either (+)- ^{11}C -McN5652 or ^{11}C -DASB must be approached with caution because of its effects on ligand metabolism and kinetics.

It has been proposed that brain cerebellar SERT binding be used as an estimate of nonspecific binding and that specific binding be calculated by subtracting cerebellar DVs from regional brain DVs (10). However, because the cerebellum is not devoid of SERT (32–36) (Fig. 5) and because binding of both radioligands decreased significantly in the cerebellum after MDMA-induced 5-HT neurotoxic injury (Tables 1 and 2; Fig. 5), this method does not appear optimal. Importantly, in the case of MDMA-induced neurotoxic injury, reductions in cortical and cerebellar binding of (+)- ^{11}C -McN5652 or ^{11}C -DASB would be missed if the proposed cerebellar subtraction method were used. Although it could be argued that binding of (+)- ^{11}C -McN5652 in some brain regions is, in fact, nonspecific and that reductions after MDMA represent a loss of some nonspecific binding site rather than loss of the SERT, this is unlikely for several reasons. First, because binding of (+)- ^{11}C -McN5652 or ^{11}C -DASB decreases significantly after MDMA treatment, one would have to postulate a nonspecific binding site with similar affinity for both radioligands. Second, the neurotoxic effects of MDMA as given to monkeys in this study are known to be highly selective toward brain 5-HT neurons (11,20–21), mitigating the possibility that reductions in binding are caused by loss of nonserotonergic neuronal elements. Third, reductions in binding of

both ligands parallel those seen *in vitro*, although, as in other brain regions, they underestimate the degree of serotonergic injury. Clearly, there is need to further develop and validate methods that provide more accurate estimates of nonspecific SERT binding in PET imaging paradigms.

It is important to note that, although the regional tissue activities and *DVs* of both radiotracers generally corresponded well with the known distribution of the SERT in the brain ($r = 0.814$ for (+)-¹¹C-McN5652 and $r = 0.843$ for ¹¹C-DASB), neither ligand modeled perfectly the *in vitro* SERT concentrations. For example, SERT density in the cerebral cortex is known to be roughly 4 times that in the cerebellum (32–34); yet binding of both ligands was similar in cortical and cerebellar tissue (Tables 1 and 2). Similarly, SERT density in the midbrain is known to be approximately twice that in the thalamus; yet binding of both radioligands in these 2 brain regions was comparable. There are several potential explanations for this phenomenon, including partial-volume effects, differential blood flow, spatial resolution of the tomographs, laminar distribution of 5-HT axons, and possible differences in tissue properties among the various brain regions analyzed. Regardless of the underlying basis for this apparent discrepancy in radioligand binding, it is important to exercise caution when comparing tissue activities or *DVs* between distinct brain regions. Rather, comparisons within a particular region, either between subjects or the same subject under different experimental conditions, would appear to be the most appropriate use for both radiotracers.

In this study, a tracer kinetic model was identified using the same approach as in a previous study (14). Statistically, the best model was the one with a single tissue compartment and 3 parameters: BV , K_1 , and k_2 . In this model, *DV* is calculated by computing the ratio of K_1 to k_2 . This model significantly improved the goodness of fit at a cost of minimal variance inflation (measured by the condition number of the parameter variance–covariance matrix). Advantages of the 3-parameter model include (a) it is robust and results in minimal variance of parameters; (b) it can be used to detect differences between untreated and MDMA-treated animals; and (c) a parameter analogous to *DV* can be obtained with the simplified graphic method, which can then be used for creation of parametric images (38). On the basis of these criteria, a single tissue compartment model with 3 parameters was used to analyze (+)-¹¹C-McN5652 and ¹¹C-DASB binding in this study. Future studies may indicate that, for both radioligands, a more complex kinetic model based on 2 tissue compartments may be more applicable. Separation of kinetic parameters at specific binding sites (e.g., k_3 and k_4) permits an independent assessment of specific binding and is expected to eliminate bias, but a more complex model will pose an additional challenge to harnessing parameter variance as the instability of the parameter estimator increases with model complexity.

It should be noted that *DV* measurements of (+)-¹¹C-McN5652 were calculated using a revised HPLC method

for analysis of plasma (+)-¹¹C-McN5652 and its metabolites, the results of which are used to correct the input function (23). With this new method, the unmetabolized fraction of (+)-¹¹C-McN5652 is higher than that with the previously published technique (12,14), resulting in much lower *DVs* and significantly lower variance (Table 2). Importantly, data collected using this refined HPLC method confirm those obtained previously (12,13), are consistent with those of others (10), and confirm that (+)-¹¹C-McN5652 is capable of detecting MDMA-induced 5-HT neuronal injury. As with measurements of cerebrospinal fluid 5-HIAA, the only other validated method for detecting MDMA-induced neurotoxicity *in vivo*, PET measurements of the SERT with either (+)-¹¹C-McN5652 or ¹¹C-DASB underestimate the extent of serotonergic injury measured postmortem, probably as a result of nonspecific ligand binding.

Potential limitations of this study should be acknowledged. First, the sample size is small. Although the sample size is indeed limited, it should be noted that each baboon was imaged 3 times with each radioligand under each experimental condition (normal SERT density, reduced SERT density, and reduced SERT availability) and that, in all cases, results were internally consistent for both ligands studied. Further, direct *ex vivo* postmortem studies confirmed that the MDMA-treated baboon did, in fact, have the expected reduced SERT density. Thus, there is little reason to suspect that our results are compromised in any significant way by the small sample size. It should be emphasized that the purpose of this study was not to establish that MDMA is neurotoxic because the neurotoxic potential of MDMA has been amply established by previous studies in this laboratory (11,13,20,21) and other laboratories (39–40). Another potential limitation is that on most, although not all, occasions, (+)-¹¹C-McN5652 was studied before ¹¹C-DASB, raising the possibility that observed differences might be related to order effects. However, on those occasions when ¹¹C-DASB was studied before (+)-¹¹C-McN5652, no obvious difference was observed, mitigating against this potential problem. Third, it was difficult to obtain a precise measure of plasma protein binding of the radioligands, particularly (+)-¹¹C-McN5652. Further refinement of the protein-binding technique and inclusion of this parameter could further improve the results of kinetic modeling. Finally, it is conceivable that the MDMA-treated animal had a smaller nonspecific distribution volume than that of the control. Although this is possible, this seems unlikely given that the animals were of similar age, weight, and sex.

CONCLUSION

Our results indicate that (+)-¹¹C-McN5652 and ¹¹C-DASB are both useful PET radioligands for the measurement of the brain SERT in living primates and that both radioligands are capable of detecting reduced SERT density secondary to MDMA-induced 5-HT neurotoxicity. Also,

both radioligands seem better suited for detecting differences of SERT binding in areas with high SERT density, such as the midbrain, thalamus, caudate, and putamen. The finding that neurotoxic injury with MDMA leads to reduced binding of (+)-¹¹C-McN5652 and ¹¹C-DASB in cortical brain regions with relatively low SERT density indicates that, in some instances, these ligands may be capable of detecting differences in neocortical SERT binding and that (+)-¹¹C-McN5652 and ¹¹C-DASB binding in cortical regions may not be entirely nonspecific. The optimal method for estimating and accounting for nonspecific binding of both ligands is not yet resolved and deserves further study because it can help reduce parameter bias as well as parameter variance. Additional studies in nonhuman primates and humans are needed to further characterize the properties and capabilities of both radioligands in healthy human beings and in individuals with neuropsychiatric disorders in which 5-HT neurons have been implicated.

ACKNOWLEDGMENTS

The authors appreciate the contribution of Jozsef Varga, PhD, who implemented and tested the software for PET-MRI registration and volumetric calculation of the tissue time-activity curves; the contributions of Robert Smoot, who assisted the cyclotron operation, radiochemistry, and radioligand quality control; and the technologists who were instrumental for the performance of the PET studies, specifically Paige A. Rauseo, David Clough, Karen Edmonds, Paul Clark, and Laura Marshall. The authors are also grateful to Dr. Levente L. Kerényi for his assistance and helpful comments. This work was supported by Public Health Service grants DA05707, DA06275, AG14400, and AA11653.

REFERENCES

- Dannals RF, Scheffel U, Suehiro M, Ricaurte G. Radioligand development for studying serotonin uptake sites with positron emission tomography. *Med Chem Res.* 1994;5:228–244.
- Jagust WJ, Eberling JL, Roberts JA, et al. *In vivo* imaging of the 5-hydroxytryptamine reuptake sites in primate brain using single photon emission tomography and [¹²³I]5-iodo-6-nitroquipazine. *Eur J Pharmacol.* 1993;242:189–193.
- Malison RT, Price LH, Berman R, et al. Reduced brain serotonin transporter availability in major depression as measured by [¹²³I]-2 beta-carbomethoxy-3 beta-(4-iodophenyl)tropane and single photon emission computed tomography. *Biol Psychiatry.* 1998;44:1090–1098.
- Oya S, Choi SR, Hou C, et al. 2-((2-(dimethylamino)methyl)phenyl)thio)-5-iodophenylamine (ADAM): an improved serotonin transporter ligand. *Nucl Med Biol.* 2000;27:249–254.
- Meltzer CC, Smith G, DeKosky ST, et al. Serotonin in aging, late-life depression, and Alzheimer's disease: the emerging role of functional imaging. *Neuropsychopharmacology.* 1998;18:407–430.
- Parsey RV, Slifstein M, Hwang DR, et al. Validation and reproducibility of measurement of 5-HT_{1A} receptor parameters with [carbonyl-¹¹C]WAY-100635 in humans: comparison of arterial and reference tissue input functions. *J Cereb Blood Flow Metab.* 2000;20:1111–1133.
- Brust P, Scheffel U, Szabo Z. Radioligands for the study of the 5-HT transporter *in vivo*. *Drugs.* 1999;2:129–145.
- Szabo Z, Kao PF, Scheffel U, et al. Positron emission tomography imaging of serotonin transporters in the human brain using [¹¹C](+)-McN5652. *Synapse.* 1995;20:37–43.
- Szabo Z, Scheffel U, Suehiro M, et al. Positron emission tomography of 5-HT transporter sites in the baboon brain with [¹¹C]McN5652. *J Cereb Blood Flow Metab.* 1995;15:798–805.
- Parsey RV, Kegeles LS, Hwang DR, et al. *In vivo* quantification of brain serotonin transporters in humans using [¹¹C]McN 5652. *J Nucl Med.* 2000;41:1465–1477.
- Scheffel U, Szabo Z, Mathews WB, et al. *In vivo* detection of short- and long-term MDMA neurotoxicity: a positron emission tomography study in the living baboon brain. *Synapse.* 1998;29:183–192.
- McCann UD, Szabo Z, Scheffel U, et al. Positron emission tomographic evidence of toxic effect of MDMA (“ecstasy”) on brain serotonin neurons in human beings. *Lancet.* 1998;352:1433–1437.
- Ricaurte GA, McCann UD, Szabo Z, Scheffel U. Toxicodynamics and long-term toxicity of the recreational drug, 3,4-methylenedioxymethamphetamine (MDMA, “ecstasy”). *Toxicol Lett.* 2000;112–113:143–146.
- Szabo Z, Scheffel U, Mathews WB, et al. Kinetic analysis of [¹¹C]McN5652: a serotonin transporter radioligand. *J Cereb Blood Flow Metab.* 1999;19:967–981.
- Buck A, Gucker PM, Schonbacher RD, et al. Evaluation of serotonergic transporters using PET and [¹¹C](+)-McN-5652: assessment of methods. *J Cereb Blood Flow Metab.* 2000;20:253–262.
- Wilson AA, Houle S. Radiosynthesis of carbon-11 labeled *N*-methyl-2-(arylthio) benzylamines: potential radiotracers for the serotonin reuptake receptor [abstract]. *J Labelled Compds Radiopharm.* 1999;42:1277.
- Wilson AA, Ginovart N, Schmidt M, et al. Novel radiotracers for imaging the serotonin transporter by positron emission tomography: synthesis, radiosynthesis, and *in vitro* and *ex vivo* evaluation of (11)C-labeled 2-(phenylthio)araalkylamines. *J Med Chem.* 2000;43:3103–3110.
- Houle S, Ginovart N, Hussey D, et al. Imaging the serotonin transporter with positron emission tomography: initial human studies with [¹¹C]DAPP and [¹¹C]DASB. *Eur J Nucl Med.* 2000;27:1719–1722.
- Meyer JH, Wilson AA, Ginovart N, et al. Occupancy of serotonin transporters by paroxetine and citalopram during treatment of depression: a [¹¹C]DASB PET imaging study. *Am J Psychiatry.* 2001;158:1843–1849.
- Fischer CA, Hatzidimitriou G, Wlos J, et al. Reorganization of ascending 5-HT axon projections in animals previously exposed to the recreational drug (+)3, 4-methylenedioxymethamphetamine (MDMA, “ecstasy”). *J Neurosci.* 1995;15:5476–5485.
- Hatzidimitriou G, McCann UD, Ricaurte GA. Altered serotonin innervation patterns in the forebrain of monkeys treated with MDMA seven years previously: factors influencing abnormal recovery. *J Neurosci.* 1999;19:5096–5107.
- Suehiro M, Ravert HT, Dannals RF, et al. Synthesis of a radiotracer for studying serotonin uptake sites with positron emission tomography: [¹¹C]McN-5652-Z. *J Labelled Compds Radiopharm.* 1992;31:841–848.
- Hilton J, Yokoi F, Dannals RF, et al. Column switching HPLC for the analysis of plasma in PET imaging studies. *Nucl Med Biol.* 2000;27:627–630.
- Rew RK, Davis GP. NetCDF: an interface for scientific data access. *IEEE Comput Graphics Applicat.* 1990;10:76–82.
- Woods RP, Cherry SR, Mazziotta JC. Rapid automated algorithm for aligning and reslicing PET images. *J Comput Assist Tomogr.* 1992;16:620–633.
- Woods RP, Mazziotta JC, Cherry SR. MRI-PET registration with automated algorithm. *J Comput Assist Tomogr.* 1993;17:536–546.
- Koeppel RA, Frey KA, Mulholland GK, et al. [¹¹C]Tropanyl benzylate-binding to muscarinic cholinergic receptors: methodology and kinetic modeling alternatives. *J Cereb Blood Flow Metab.* 1994;14:85–99.
- Marquardt DW. An algorithm for least-squares estimation of nonlinear parameters. *J Soc Indust Appl Math.* 1963;11:431–441.
- Ricaurte G, Martello AL, Katz JL, Martello MB. Lasting effects of (+)-3,4-methylenedioxymethamphetamine (MDMA) on central serotonergic neurons in nonhuman primates: neurochemical observations. *J Pharmacol Exp Ther.* 1992;261:616–622.
- Bailey D. Tables of the Bonferroni *t* statistics. *J Am Stat Assoc.* 1977;72:469–478.
- Muzik O, Chugani DC, Chakraborty PK, et al. Analysis of C-11 alpha-methyltryptophan kinetics for the estimation of serotonin synthesis rate *in vivo*. *J Cereb Blood Flow Metab.* 1997;17:659–669.
- Cortés R, Soriano E, Pazos A, et al. Autoradiography of antidepressant binding sites in the human brain: localization using [³H]imipramine and [³H]paroxetine. *Neuroscience.* 1988;27:473–496.
- Laruelle M, Vanisberg M-A, Maloteaux J-M. Regional and subcellular localization in human brain of [³H]paroxetine binding, a marker of serotonin uptake sites. *Biol Psychiatry.* 1988;24:299–309.
- Bäckström I, Bergström M, Marcusson J. High affinity [³H]paroxetine binding to serotonin uptake sites in human brain tissue. *Brain Res.* 1989;486:261–268.
- Fuxe K, Agnati LF, Bjelke B, et al. Novel aspects on central 5-hydroxytryptamine neurotransmission: focus on the cerebellum. In: Trouillas P, Fuxe K, eds. *Serotonin, the Cerebellum, and Ataxia*. New York, NY: Raven Press; 1993:1–37.

36. Bishop GA, Kerr CW, Chen YF, King JS. The serotonergic system in the cerebellum: origin, ultrastructural relationships, and physiological effects. In: Trouillas P, Fuxe K, eds. *Serotonin, the Cerebellum, and Ataxia*. New York, NY: Raven Press; 1993:91–112.
37. Landaw EM, DiStefano JJ. Multiexponential, multicompartamental, and noncompartmental modeling. II. Data analysis and statistical considerations. *Am J Physiol*. 1984;246:R665–R677.
38. Logan J, Fowler JS, Volkow D, et al. Graphical analysis of reversible radioligand binding from time-activity measurements applied to [N - ^{11}C -methyl]-(-)-cocaine PET studies in human species. *J Cereb Blood Flow Metab*. 1990;10:740–747.
39. Steele T, McCann U, Ricaurte G. 3-Dimensional, 4-methylenedioxymethamphetamine (MDMA, “ecstasy”): pharmacology and toxicology in animals and humans. *Addiction*. 1994;89:539–551.
40. Insel TR, Battaglia G, Johannessen JN, et al. (+)3,4-Methylenedioxymethamphetamine (MDMA, “ecstasy”) selectively destroys brain serotonin terminals in rhesus monkey. *J Pharmacol Exp Ther*. 1989;249:713–720.

